NATIONAL INSTITUTE FOR FUSION SCIENCE

Current-Induced Cooling Phenomenon in a Two-Dimensional Electron Gas under a Magnetic Field

N. Hirayama, A. Endo, K. Fujita, Y. Hasegawa, N. Hatano,
H. Nakamura, R. Shirasaki and K. Yonemitsu

(Received - June 15, 2011)

NIFS-1016 June 22, 2011

RESEARCH REPORT
NIFS Series

TOKI, JAPAN

Current-Induced Cooling Phenomenon in a Two-Dimensional Electron Gas under a Magnetic Field

Naomi Hirayama,[1] Akira Endo,[2] Kazuhiro Fujita,[2] Yasuhiro Hasegawa,[3]
Naomichi Hatano,[1] Hiroaki Nakamura,[4] Ryōen Shirasaki,[5] and Kenji Yonemitsu[6]

[1]*Institute of Industrial Science, University of Tokyo, 4-6-1 Komaba, Meguro, Tokyo 153-8505, Japan*
[2] *Institute for Solid State Physics, University of Tokyo, 5-1-5 Kashiwanoha, Kashiwa, Chiba 277-8581, Japan*
[3]*Department of Environmental Science and Technology, Saitama University, 255 Shimo-Okubo, Sakura-ku, Saitama City, Saitama 338-8570, Japan*
[4]*Fundamental Physics Simulation Research Division, National Institute for Fusion Science, Oroshi-cho, Toki, Gifu, 509-5292, Japan*
[5]*Department of Physics, Yokohama National University, 79-5 Tokiwadai, Hodogaya-ku, Yokohama 240-8501, Japan*
[6]*Department of Theoretical and Computational Molecular Science, Institute for Molecular Science, 38 Nishigo-Naka, Myodaiji, Okazaki 444-8585, Japan*

(Dated: June 15, 2011)

We investigate the spatial distribution of temperature induced by a dc current in a two-dimensional electron gas (2DEG) subjected to a perpendicular magnetic field. We numerically calculate the distributions of the electrostatic potential ϕ and the temperature T in a 2DEG enclosed in a square area surrounded by insulated-adiabatic (top and bottom) and isopotential-isothermal (left and right) boundaries (with $\phi_{\rm left} < \phi_{\rm right}$ and $T_{\rm left} = T_{\rm right}$), using a pair of nonlinear Poisson equations (for ϕ and T) that fully take into account thermoelectric and thermomagnetic phenomena, including the Hall, Nernst, Ettingshausen, and Righi-Leduc effects. We find that, in the vicinity of the left-bottom corner, the temperature becomes lower than the fixed boundary temperature, contrary to the naive expectation that the temperature is raised by the prevalent Joule heating effect. The cooling is attributed to the Ettingshausen effect at the bottom adiabatic boundary, which pumps up the heat away from the bottom boundary. In order to keep the adiabatic condition, a downward temperature gradient, hence the cooled area, is developed near the boundary, with the resulting thermal diffusion compensating the upward heat current due to the Ettingshausen effect.

Keywords: magnetothermoelectric effect, transport equation, nonlinear Poisson equation, finite difference method, two dimensional electron gas, Ettingshausen effect, cooling phonomenon

I. INTRODUCTION

The thermoelectric and thermomagnetic phenomena[1] have recently been attracting renewed interest not only as a route for potentially highly efficient device application, e.g., in refrigeration or generating electricity, but also as an effective tool to explore fundamental properties of solid-state materials.[2–5] Being sensitive to the energy derivative of the electric conductivity (or of the density of states) or to the entropy of the system, the thermoelectric and thermomagnetic properties provide us with the information on the materials complementary to, and often with higher sensitivity than, the electric conductivity.[6–14] For instance, it has been shown that the Seebeck or Nernst coefficient measured in a bismuth single crystal[12,13] or a two-dimensional electron gas (2DEG)[14] exhibits clearer quantum oscillations due to the Landau quantization compared to those of the electric conductivity (the Shubnikov-de Haas oscillations). The thermoelectric effects also bring about an additional twist to the measurement of the electric conductivity or the resistivity, or more generally to the distribution of the electrostatic potential and the electric current. For example, it is necessary to take into consideration the thermovoltages in the precision resistivity measurement.[15] Further complication arises by the application of a magnetic field.[16–19] Nontrivial distributions of the potential and the current, and hence the temperature, can be generated by the thermoelectric and thermomagnetic effects.

Fujita *et al.*[20] recently reported an anomalous behavior of the Nernst signal in a quantum Hall system, which suggests possible cooling of the electron temperature by the current intended to heat the electron system to introduce the temperature gradient. Figure 1 (a) shows a schematic diagram of the experimental device. The top (horizontal) bar is used as a heater; Joule heating by the heating current $I_h = 4$ nA/μm supposedly raises the electron temperature $T_{\rm e,high}$ there and introduces a temperature gradient toward the Ohmic contact pad below. The pad is thermally connected to the mixing chamber of the dilution fridge kept at $T_{\rm e,low} = 40$ mK, in which the sample is immersed. Thermoelectric voltages are measured in the main (vertical) Hall bar. Arms to measure the transverse thermoelectric (Nernst) voltage V_{yx} are shown in the figure. Note that with this current heating technique, one can heat up the electron temperature selectively, leaving the lattice temperature intact (so long as I_h is kept low enough). Therefore, one can pick out the diffusion contribution in the thermoelectric voltages[21] and can eliminate the phonon-drag contribution, which

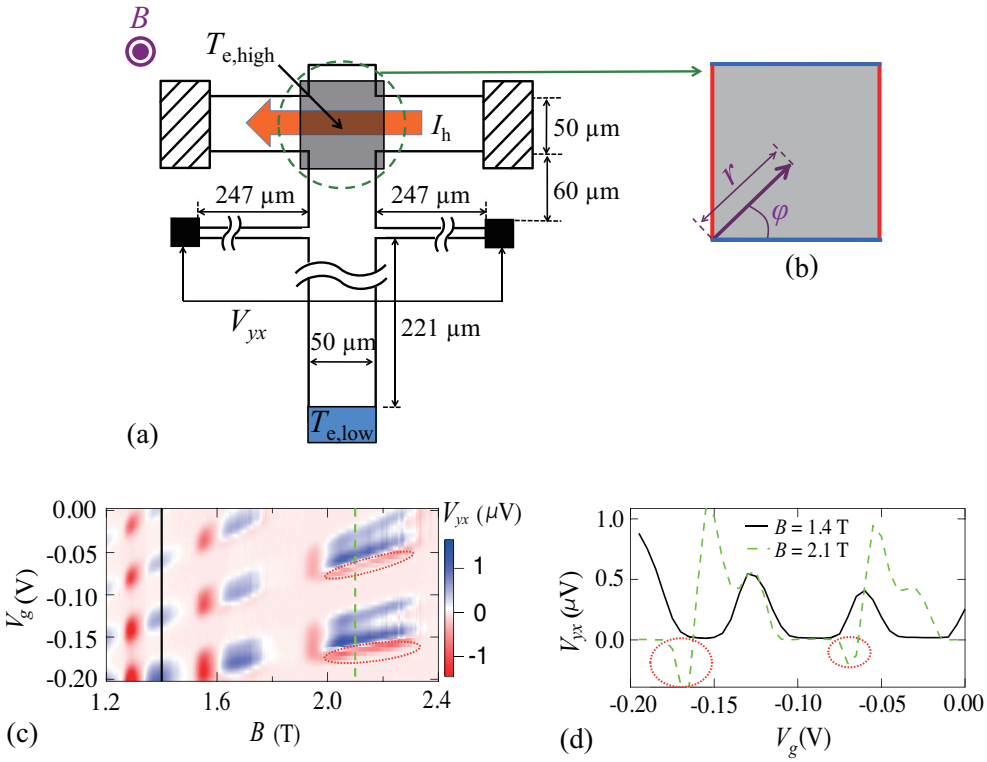

FIG. 1: (a) Schematic drawing of the experimental device[20]. A magnetic field B is perpendicular to the 2DEG plane. The Nernst voltage V_{yx} is measured between the probes indicated as the black squares. The gray square indicates the front gate. The current $I_h = 4$ nA/μm supposedly heats the region underneath the front gate to $T_{\rm e,high}$ and introduces a temperature gradient toward the bottom pad held at $T_{\rm e,low} = 40$ mK. (b) Geometry used in the calculation to approximate the heater section (section beneath the top gate). Top and bottom (blue) boundaries are assumed to be insulated and adiabatic, while left and right (red) edges have a fixed potential and a temperature, $\phi_{\rm left} = 0$ nV, $\phi_{\rm right} = 80$ nV, $T_{\rm left} = T_{\rm right} = 40$ mK. We introduce the polar coordinates (r, φ) with the origin located at the left-bottom corner. (c) Color plot of experimentally obtained Nernst voltage V_{yx} in the plane of B and applied gate voltage V_g, with blue and red colors representing the positive and the negative value, respectively. (d) Cross sections indicated by solid and dashed vertical lines in (c). Anomalous behavior discussed in the text is highlighted by dotted ellipses in (c) and (d).

is often the dominant contribution in the thermoelectric powers in a 2DEG.[5] The (negative) gate voltage V_g applied to the front gate (shown by the gray square in Fig. 1 (a)) allows us to control the carrier density and hence the resistance of the heater section independently from the main Hall bar. Figure 1 (c) shows the Nernst voltage V_{yx} plotted in the B-V_g plane. Thermoelectric voltages vanish when the 2DEG is in the quantum Hall states[5,22,23] and Joule heating does not work when the heater section is in the dissipationless state. Therefore, nonvanishing signal appears only when both the main Hall bar and the heater section are in between two adjacent quantum Hall states, namely only when the Fermi energies (E_F) of the both sections cross (disorder-broadened) Landau levels having finite density-of-states.

Below $B = 1.8$ T, the Nernst voltage V_{yx} behaves as expected, showing oscillations as a function of B (taking negative then positive values when E_F of the main Hall bar crosses a Landau level)[22,24], but does not depend much on V_g insofar as the heater section is in the dissipative states. Note that V_g alters only the heater section and should have no effect on the main Hall bar (the section where the thermoelectric voltages are measured). Anomalous behaviors are observed above 1.8 T: V_{yx} alternates the sign when V_g is swept at a fixed B (see Fig. 1 (d)). Negative V_{yx} appears for smaller (more negative) V_g at the higher magnetic field side where V_{yx} is expected to be positive (the areas indicated by dotted ellipses in Fig. 1 (c) and (d)). The inversion in the sign of V_{yx} can be naively interpreted as resulting from the inversion in the sign of the temperature gradient, implying that the "heater" section can actually be cooled by I_h, depending on the value of V_g. This speculation led us to investigate the current-induced temperature distribution of a 2DEG placed in a magnetic field, in pursuit of the possibility of the current-induced cooling.

In the present paper, we numerically examine the spatial distribution of the temperature T in a segment of 2DEG that simulates the heater section of the experimental device, fully taking the thermoelectric and ther-

momagnetic effects into account. In order to focus on the current-induced cooling, we leave out the main Hall bar altogether and approximate the heater section as a square surrounded by insulated-adiabatic (top and bottom) and isopotential-isothermal (left and right) boundaries[25] in the calculation, as shown in Fig. 1 (b). We basically follow the prescription presented by Okumura and coauthors[26] for 3D semiconductors at the room temperature and extend their treatment to a 2DEG at low temperatures. In this treatment, the contributions of the phonons are neglected, which is justified at the extremely low temperature (40 mK) considered in the present paper. The distributions of the electrostatic potential ϕ (with the electrochemical potential given by $-e\phi$, see the discussion below) and the temperature T are obtained by solving the nonlinear Poisson equations, $\nabla^2\phi = F(T, \nabla T, \nabla\phi)$ and $\nabla^2 T = G(T, \nabla T, \nabla\phi)$, with the functions G and F derived from the transport equations[1,26–29], as detailed in section II. We find that a magnetic field distorts equi-potential lines and generates an uneven temperature distribution with high- and low-temperature areas emerging at the opposite corners of the square (see Fig. 3 below). The low-temperature area is found to become colder than the isothermal boundaries. A similar phenomenon was previously reported by Ise *et al.*,[18] although the origin of the cooling was not explicitly specified then. The emergence of the cooled part possibly gives a qualitative account of the experimentally observed sign reversal in the Nernst signal[20] mentioned above.

The main purpose of the present paper is to clarify the mechanism of this cooling effect. We numerically evaluate the terms in the right-hand sides F and G of the nonlinear Poisson equations and identify the dominant terms that induce the cooling. We find that the cooling is mainly attributable to the adiabatic condition for the bottom edge. It causes a temperature gradient and hence the thermal diffusion to cancel the heat current away from the edge deriving from the Ettingshausen effect, and consequently generates the cooled area adjacent to the edge.

The paper is organized as follows. In section II, we describe the method of calculating the spatial distributions of ϕ and T by solving the nonlinear Poisson equations followed by the results of the simulation. In section III, we discuss the mechanism of the partial cooling through the identification of the dominant terms in the equations. In Section IV, we discuss our results in connection with the experiment that motivated our study. Section V is devoted to conclusions.

II. NUMERICAL CALCULATION

The transport equations describing the electric current density $\boldsymbol{J}$ and the thermal current density $\boldsymbol{J_Q}$ for isotropic systems[1,26–29] are:

$$-\nabla\phi = \rho\boldsymbol{J} + R(\boldsymbol{B}\times\boldsymbol{J}) + \alpha\nabla T + N(\boldsymbol{B}\times\nabla T), \quad (1)$$

$$\boldsymbol{J_Q} = \alpha T\boldsymbol{J} + NT(\boldsymbol{B}\times\boldsymbol{J}) - \kappa\nabla T + \kappa M(\boldsymbol{B}\times\nabla T), \quad (2)$$

where $\boldsymbol{B}$ denotes the magnetic field, ρ the electric resistivity, R the Hall coefficient, α the Seebeck coefficient, N the Nernst coefficient, κ the thermal conductivity, and M the Righi-Leduc coefficient. The transport coefficients, ρ, R, α, N, κ, and M are all defined in the isothermal conditions. The terms on the right-hand sides of Eqs. (1) and (2) respectively represent transport phenomena as follows: Ohm's law, the Hall effect, the Seebeck effect, and the Nernst effect in Eq. (1); the Peltier effect, the Ettingshausen effect, Fourier's law of the thermal conductivity, and the Righi-Leduc effect in Eq. (2).

We define the energy-flux density $\boldsymbol{J_U}$ as

$$\boldsymbol{J_U} = \boldsymbol{J_Q} + \phi\boldsymbol{J}. \quad (3)$$

Here we selected the Fermi level (chemical potential at $T = 0$) as the origin of the energy. Because the temperature dependence of the chemical potential is negligibly small at the low temperatures considered in the present paper, the electrochemical potential is given by $-e\phi$, hence the definition Eq. (3). From Eqs. (1)–(3) and the equations of continuity in the steady state $\nabla\cdot\boldsymbol{J} = \nabla\cdot\boldsymbol{J_U} = 0$, we obtain the nonlinear Poisson equations (see Appendix A for the derivation),

$$\begin{aligned}\nabla^2\phi = {}& \rho C(T) J^2 \\ & - \left[\frac{d\alpha}{dT} + \frac{RB^2}{\rho}\frac{dN}{dT} + C(T)\left(\frac{NB^2T}{\rho}\frac{dN}{dT} - \frac{d\kappa}{dT}\right)\right] (\nabla T)^2 \\ & + \left[\frac{R}{\rho}\frac{d\rho}{dT} - \frac{dR}{dT} - C(T)\left(T\frac{dN}{dT} + 2N - \frac{NT}{\rho}\frac{d\rho}{dT}\right)\right] [(\boldsymbol{B}\times\boldsymbol{J})\cdot\nabla T] \\ & - \left[\frac{d\rho}{dT} + \frac{RB^2}{\rho}\frac{dR}{dT} + C(T)\left(T\frac{d\alpha}{dT} + \frac{NB^2T}{\rho}\frac{dR}{dT}\right)\right] (\boldsymbol{J}\cdot\nabla T) \\ \equiv {}& F(T, \nabla T, \nabla\phi), \end{aligned} \quad (4)$$

$$C(T) = \frac{\alpha\rho + RNB^2}{\rho\kappa - N^2B^2T}, \quad (5)$$

$$\begin{aligned}\nabla^2 T = {}& \frac{\rho}{\rho\kappa - N^2B^2T} \\ & \times \left\{-\rho J^2 + \left(\frac{NB^2T}{\rho}\frac{dN}{dT} - \frac{d\kappa}{dT}\right)(\nabla T)^2 \right. \\ & + \left(T\frac{dN}{dT} + 2N - \frac{NT}{\rho}\frac{d\rho}{dT}\right)[(\boldsymbol{B}\times\boldsymbol{J})\cdot\nabla T] \\ & \left. + \left(T\frac{d\alpha}{dT} + \frac{NB^2T}{\rho}\frac{dR}{dT}\right)(\boldsymbol{J}\cdot\nabla T)\right\} \\ \equiv {}& G(T, \nabla T, \nabla\phi). \end{aligned} \quad (6)$$

The electric current $\boldsymbol{J} = (J_x, J_y)$ to be replaced in Eqs. (4) and (6) is obtained by inverting Eq. (1):

$$\begin{pmatrix} J_x \\ J_y \end{pmatrix} = \frac{1}{\rho^2 + R^2B^2} \begin{pmatrix} \rho & RB \\ -RB & \rho \end{pmatrix} \times \begin{pmatrix} -\partial_x\phi - \alpha\partial_x T + NB\partial_y T \\ -\partial_y\phi - \alpha\partial_y T - NB\partial_x T \end{pmatrix}. \quad (7)$$

As illustrated in Fig. 1 (b), the left and the right edges

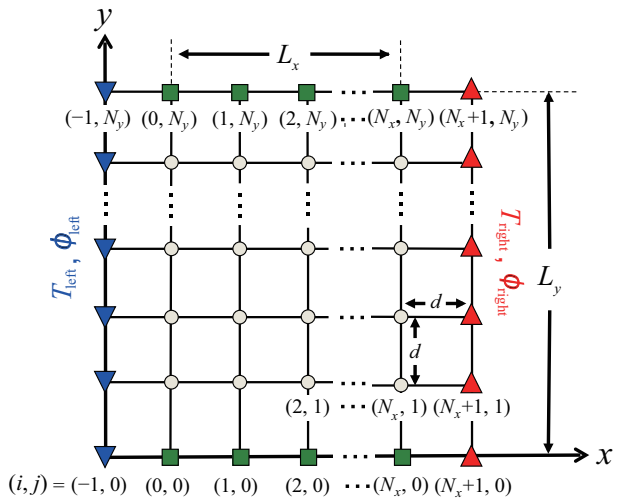

FIG. 2: (Color online) Discretized two-dimensional sample, where the sample size is $L_x = L_y = 10\,\mu$m and the mesh size is $d = 0.1\,\mu$m. Thus, the number of the grid points is $(N_x+1)\times(N_y+1) = 101\times101$. The label (i, j) denotes the (i, j)th grid point along the x- and y-axes, respectively. The downward (blue) and upward (red) triangles on $i = -1$ and on $i = N_x+1$ have potentials and temperatures fixed to $(\phi_{\rm left}, T_{\rm left})$ and $(\phi_{\rm right}, T_{\rm right})$, respectively, set as $\phi_{\rm left} = 0$ nV and $\phi_{\rm right} = 80$ nV, $T_{\rm left} = T_{\rm right} = 40$ mK. The (green) squares on the top and bottom boundaries are insulated and adiabatic. The magnetic field $\boldsymbol{B}$ is perpendicular to the sample.

are isopotential and isothermal, i.e., ϕ and T are fixed (the Dirichlet conditions). On the top and the bottom edges, we set the insulated and adiabatic conditions; the normal components of $\boldsymbol{J}$ and $\boldsymbol{J_Q}$ vanish at these boundaries. Let us denote the quantities at the boundaries with tilde, $\widetilde{\phi}$, $\widetilde{\boldsymbol{J}}$, $\widetilde{T}$, and $\widetilde{\boldsymbol{J}}_{\boldsymbol{Q}}$. Equations (1) and (2) at the boundaries are then reduced to

$$-\partial_x\widetilde{\phi} = \rho\widetilde{J}_x + \alpha\partial_x\widetilde{T} - NB\partial_y\widetilde{T}, \quad (8a)$$

$$-\partial_y\widetilde{\phi} = RB\widetilde{J}_x + \alpha\partial_y\widetilde{T} + NB\partial_x\widetilde{T}, \quad (8b)$$

$$0 = NTB\widetilde{J}_x - \kappa\partial_y\widetilde{T} + \kappa MB\partial_x\widetilde{T}. \quad (8c)$$

We thus obtain the following derivatives (the Neumann conditions),

$$\partial_y\widetilde{\phi} = -\left(R + \frac{\alpha NT}{\kappa}\right)B\widetilde{J}_x - (\alpha M + N)B\partial_x\widetilde{T}, \quad (9a)$$

$$\partial_y\widetilde{T} = \frac{NTB}{\kappa}\widetilde{J}_x + MB\partial_x\widetilde{T}, \quad (9b)$$

where the electric current $\widetilde{J}_x$ on the boundary is given by

$$\widetilde{J}_x = -\frac{\kappa}{\rho\kappa - N^2B^2T}\left[\partial_x\widetilde{\phi} + (\alpha - MNB^2)\partial_x\widetilde{T}\right]. \quad (9c)$$

We numerically solve the set of equations (4) and (6) self-consistently on a discretized sample illustrated in Fig. 2. We employ the successive over-relaxation (SOR) method[30,31] in the finite-difference calculations to achieve high efficiency in the convergence. We compute in our discretized calculation the y-derivatives of ϕ and T on the top and bottom boundaries with the use of the expressions in Eq. (9) in terms of the x-derivatives, which can be easily evaluated by finite differences.[30–32] The full account of the algorithm is provided in Ref. 32.

We found that the convergence of the calculation is very poor for larger values of B, despite the use of the SOR method. We therefore used the following strategy. We started our calculation without a magnetic field, giving the initial distributions of ϕ and T as linear functions between the left and right isopotential-isothermal boundaries. Once we reached the convergence, we then increased B from 0 to 10^{-3} T and sought the convergence. We successively increased B step by step with an increment of 10^{-3} T, using the result for the previous value of B as the initial distribution for the next value of B. Nevertheless, we have so far reached only up to 0.2 T, the convergence becoming increasingly slower with increasing magnetic field.

We performed the calculations with the parameters listed in Table I: ρ and R are taken from the experimental data[20] and other parameters, α, N, κ, M, and their temperature derivatives, are calculated, for lack of reliable experimental data for the diffusion contribution, by substituting the values of ρ and R into the semiclassical formulas[5] (for α and N) and making use of the Wiedemann-Franz law [33] (for κ and M), which is valid for the diffusion contribution. As an initial step, we used the values of the parameters at $B = 0$ throughout the calculation in the present study, neglecting their magnetic-field dependence. Although this appears to be very crude approximation, the parameters at $B = 0$ represent roughly the right order of magnitude for their values under a finite B when the Fermi energy E_F crosses the Landau levels (by contrast, some of the parameters vanish in the quantum Hall states). We hence believe that they suffice to discuss qualitatively what happens when the heater section is in the dissipative regime.

Figure 3 shows the distributions of the electrostatic potential ϕ, the electric current $\boldsymbol{J}$, the temperature T, and the heat current $\boldsymbol{J_Q}$ in the case $\phi_{\rm left} = 0$ nV, $\phi_{\rm right} = 80$ nV, and $T_{\rm left} = T_{\rm right} = 40$ mK. (We briefly reported the numerical results shown here in our previous articles.[34,35]) At $B = 0$ (Fig. 3 (a)) the electric current $\boldsymbol{J}$ flows homogeneously and perpendicularly to the ϕ-contours. The temperature, raised by the Joule heating, has a symmetric distribution decreasing towards the left and right edges held at the fixed temperature. The

TABLE I: Parameters used for the calculation.

Parameter	Value	Parameter	Value
Resistivity ρ	20.0 Ω^a	$d\rho/dT$	1 nΩK$^{-1\,c}$
Hall coefficient R	-1600.0 ΩT$^{-1\,a}$	dR/dT	1 nΩT^{-1}K$^{-1\,c}$
Seebeck coefficient α	-0.175 μVK$^{-1\,b}$	$d\alpha/dT$	-4.38 μVK$^{-2\,b}$
Nernst coefficient N	-7.35 μVK^{-1}T$^{-1\,b}$	dN/dT	-184 μVK^{-2}T$^{-1\,b}$
Thermal conductivity κ	42.7 pWK$^{-1\,b}$	$d\kappa/dT$	1 nWK$^{-2\,b}$
Righi-Leduc coefficient M	-70.0 m^{2}V^{-1}s$^{-1\,b}$	dM/dT	0^b

[a]Experimental parameters taken from Ref. 20.
[b]Values calculated with experimentally obtained ρ and R by the semiclassical theory, at $T = 40$ mK, assuming that the scattering time τ depends on the energy ε as $\tau \propto \varepsilon^{1.5}$.
[c]Tentative values for the numerical calculation, assumed to be small enough not to affect the result of the calculation.

asymmetry of the heat current J_Q, with the net flow going to the right, arises because of the left-going potential energy flow due to J (the second term in Eq. (3)). Once the magnetic field is switched on (Fig. 3 (b)–(d)), the ϕ-contour is distorted. The current J flows nearly parallel to the ϕ-contours, or more precisely, approximately at the Hall angle

$$\theta_{\rm H} = -\arctan\left(\frac{RB}{\rho}\right), \tag{10}$$

deflected from the gradient $\nabla\phi$. The Hall angle $\theta_{\rm H}$ equals 76°, 83°, and 86° at $B = 0.05$ T, 0.1 T, and 0.2 T, respectively. The current J is highly concentrated at the right-top and left-bottom corners (see also Fig. 4). The distributions of ϕ and J are qualitatively the same as well-known distributions calculated without taking the thermoelectric and thermomagnetic effects into consideration.[36–39] More quantitative comparison will be made in Sec. III A. The temperature distribution becomes asymmetric, with high and low-temperature parts emerging around the right-top and left-bottom corners, respectively (where J has a high concentration). The low-temperature part has temperatures lower than the temperature $T_{\rm left} = T_{\rm right}$ of the heat baths. We will show in Sec. III C that, in principle, the cooling appears with an arbitrarily small magnetic field.

III. MECHANISM OF THE COOLING PHENOMENON

In the present section, we investigate the origin of the cooling effect.

A. Simplification of the governing equations

As an initial step toward the understanding of the cooling mechanism, we deduce an approximate version of the governing equations and the boundary conditions much simpler than the original ones. To this end, we compare the terms in the relevant equations using the numerical solutions presented in the previous section and eliminate the terms whose contributions are negligibly small compared to the other terms. First, in Eq. (1), we find that $|\alpha\nabla T|/|\nabla\phi| \lesssim 10^{-5}$ and $|NB \times \nabla T|/|\nabla\phi| \lesssim 10^{-6}$ in the magnetic field range examined in the present paper. Therefore the terms $\alpha\nabla T$ and $NB\nabla T$ can safely be neglected. Noting that $d\rho/dT$ and dR/dT are also negligibly small in a 2DEG at $T < 0.1$ K, we arrive at the Laplace equation,

$$\nabla^2\phi = 0, \tag{11}$$

for the electrostatic potential and the expression

$$\begin{pmatrix} J_x \\ J_y \end{pmatrix} = \frac{1}{\rho^2 + R^2B^2}\begin{pmatrix} \rho & RB \\ -RB & \rho \end{pmatrix}\begin{pmatrix} -\partial_x\phi \\ -\partial_y\phi \end{pmatrix}. \tag{12}$$

for the current, as simplified equations to take the place of Eqs. (4) and (7), respectively. We can thus calculate with high accuracy the distributions of ϕ and J neglecting the thermoelectric and thermomagnetic effects. This is to be expected since we adopted rather large potential difference but no difference in the temperature between left and right edges as the boundary condition. Since the Laplace equation (11) can be solved analytical for our boundary conditions[37] (see Sec. III C), this approximation vastly simplifies the calculation.

Next we examine Eq. (6). We find that the term including ρJ^2 (corresponding to the Joule heating) is by far the dominant term, exceeding the other terms by factor 10^6. Along with $N^2B^2T/\rho\kappa \sim O(10^{-16})$, we have

$$\nabla^2 T = -\frac{\rho}{\kappa}J^2, \tag{13}$$

as a simplified approximate nonlinear Poisson equation for the temperature.

The boundary conditions (8) at the top and bottom boundaries can also be simplified as

$$-\partial_x\widetilde{\phi} = \rho\widetilde{J}_x, \tag{14a}$$

$$-\partial_y\widetilde{\phi} = RB\widetilde{J}_x, \tag{14b}$$

$$0 = NTB\widetilde{J}_x - \kappa\partial_y\widetilde{T} + \kappa MB\partial_x\widetilde{T}. \tag{14c}$$

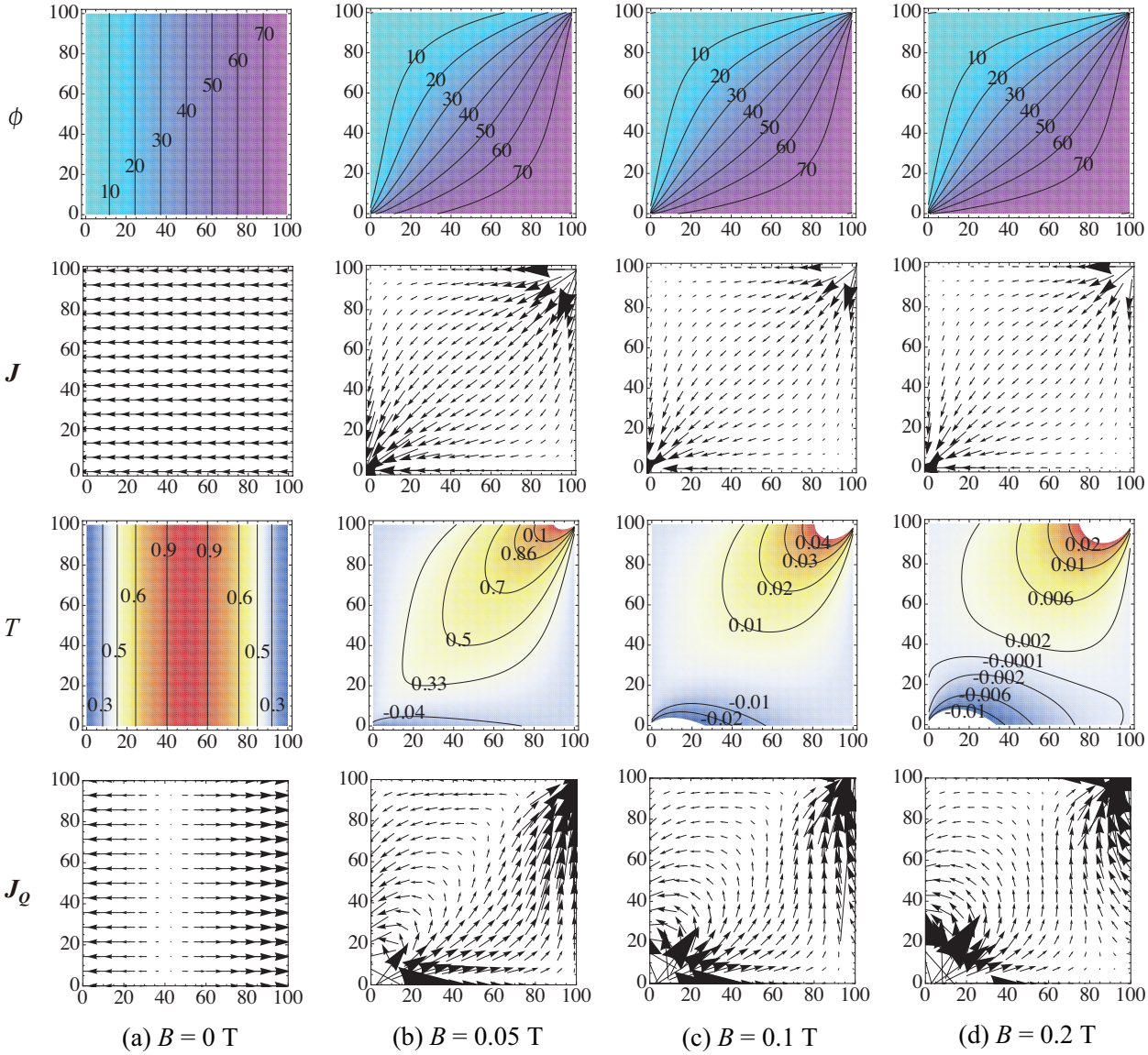

FIG. 3: (Color online) Distributions of ϕ, $\boldsymbol{J}$, T and $\boldsymbol{J_Q}$ obtained from the nonlinear Poisson equations (4) and (6) with the boundary conditions $\phi_{\rm left} = 0.0$ nV, $\phi_{\rm right} = 80$ nV and $T_{\rm left} = T_{\rm right} = 40$ mK. The ϕ-contours are labeled by the values in the unit of nanovolt, and the T-contours by the difference from $T_{\rm left} = T_{\rm right}$ in the unit of microkelvin. (a) $B = 0.0$ T. The potential gradient generates a uniform current distribution and the resulting Joule heat raises the temperature in the mid part. (b)–(d) The magnetic field causes the distortion of the equi-potential lines and the distribution of the electric current $\boldsymbol{J}$. It also affects the distribution of the temperature T and generates the area having the temperature lower than the temperature of the heat baths. The cooled area occurs, in principle, with an arbitrarily small magnetic field, although it is apparent above 0.03 T in our discretized sample. (See Sec. III C for discussion).

(Note that Eq. (14c) is the same as Eq. (8c) because all the terms are of comparable orders and therefore cannot be neglected.) Equivalently, we have the Neumann condition

$$\partial_y \widetilde{\phi} = -RB\widetilde{J}_x, \tag{15a}$$

$$\partial_y \widetilde{T} = \frac{NTB}{\kappa}\widetilde{J}_x + MB\partial_x \widetilde{T}, \tag{15b}$$

$$\widetilde{J}_x = -\frac{1}{\rho}\partial_x \widetilde{\phi}. \tag{15c}$$

(See Ref. 32 for the details of the numerical comparison of the terms.) As can be seen from Eq. (13), the spatial variation of the temperature in the interior of the sample is mainly determined by the Joule heating, the thermoelectric and thermomagnetic effects playing only minor roles. This is not the case at the boundaries, where the adiabaticity is achieved among the Ettingshausen effect, thermal diffusion, and the Righi-Leduc effect, as can be seen in Eq. (14c).

To confirm the appropriateness of the simplification,

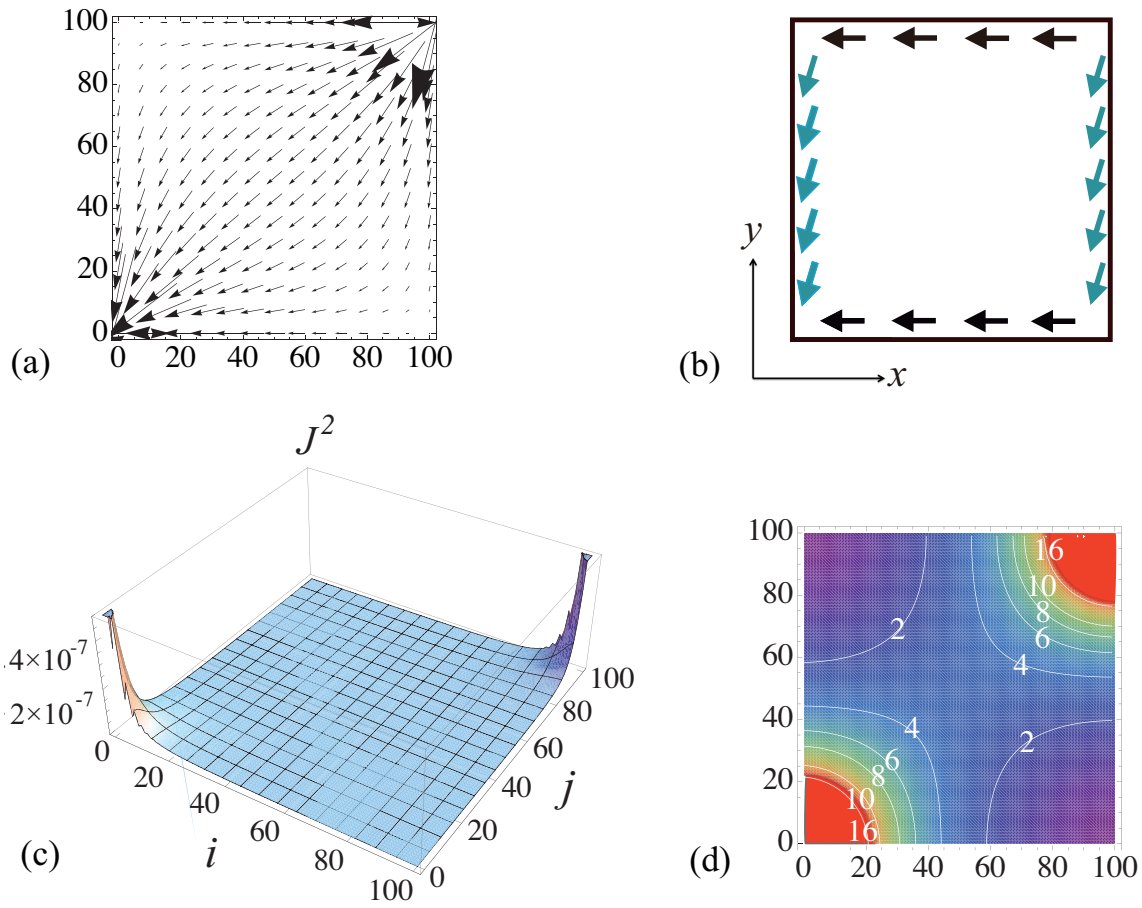

FIG. 4: (Color online) (a) Distribution of $\boldsymbol{J}$. (b) Schematic view of $\boldsymbol{J}$ on the boundaries. (c) Distribution of J^2. (d) Contour lines of J^2 in units of nA^2. All data for $B = 0.1$ T.

we calculated ϕ, $\boldsymbol{J}$, T, $\boldsymbol{J_Q}$ with the simplified equations (11)–(13) and (15) and obtained the distribution virtually indistinguishable from Fig. 3. The relative differences $\delta A = |(A - A')/A|$, where A and A' are the values from the original and the simplified equations, respectively, were sufficiently small for ϕ, T, $\boldsymbol{J}$, and $\boldsymbol{J_Q}$ as $\delta\phi \lesssim O(10^{-5})$, $\delta T \lesssim O(10^{-10})$, $\delta J_x \lesssim O(10^{-6})$, $\delta J_y \lesssim O(10^{-6})$, $\delta J_{Qx} \lesssim O(10^{-7})$, and $\delta J_{Qy} \lesssim O(10^{-7})$. It verifies that the simplified equations (11)–(13) and (15) effectively give the same distributions as those from the original equations (4)–(7) and (9).

B. The role of the Ettingshausen and the Righi-Leduc effect

In this section, we examine the role played by the first and the third terms in Eq. (14c) (the Ettingshausen and Righi-Leduc effects). We substitute 0 for the coefficients N and/or M, in order to see which term is responsible for the appearance of the cooled area. We thereby confirm that it is the Ettingshausen effect at the boundary that is indispensable for the cooling effect.

First, we consider the case $N = M = 0$ in Eq. (14c); that is, $\partial_y \widetilde{T} = 0$ at the top and the bottom boundaries. Figure 5 (a) shows the distributions of ϕ, $\boldsymbol{J}$, T and $\boldsymbol{J_Q}$ in this case. The result shows that the right-top and the left-bottom corners have much higher temperatures than elsewhere owing to the Joule heating by the highly concentrated electric-current density J illustrated in Fig. 4.

Next, we assume that $N \neq 0$ and $M = 0$ in Eq. (14c), or $0 = NTB\widetilde{J}_x - \kappa\partial_y\widetilde{T}$. In this case, we obtain a cooled area, as shown in Fig. 5 (b). It is obvious, therefore, that the first term in Eq. (14c) plays a major role in the cooling. The temperatures on the top (bottom) boundary are now higher (lower) compared with those in Fig. 5 (a). This change in the temperature map results from an upward temperature gradient $\partial_y\widetilde{T} = (NTB/\kappa)\widetilde{J}_x$ on the adiabatic boundaries (with the negative value of N). The temperature gradient can be viewed as being generated in order that the resulting downward thermal diffusion may cancel the upward heat current brought about by the Ettingshausen effect on the adiabatic boundary, as illustrated in Fig. 6. If we set, in turn, $N = 0$, $M \neq 0$ in Eq. (14c), i.e., $0 = -\partial_y\widetilde{T} + MB\partial_x\widetilde{T}$, the cooling effect does not appear as seen in Fig. 5 (c). The boundary condition yields a downward gradient $\partial_y\widetilde{T} = MB\partial_x\widetilde{T}$, with

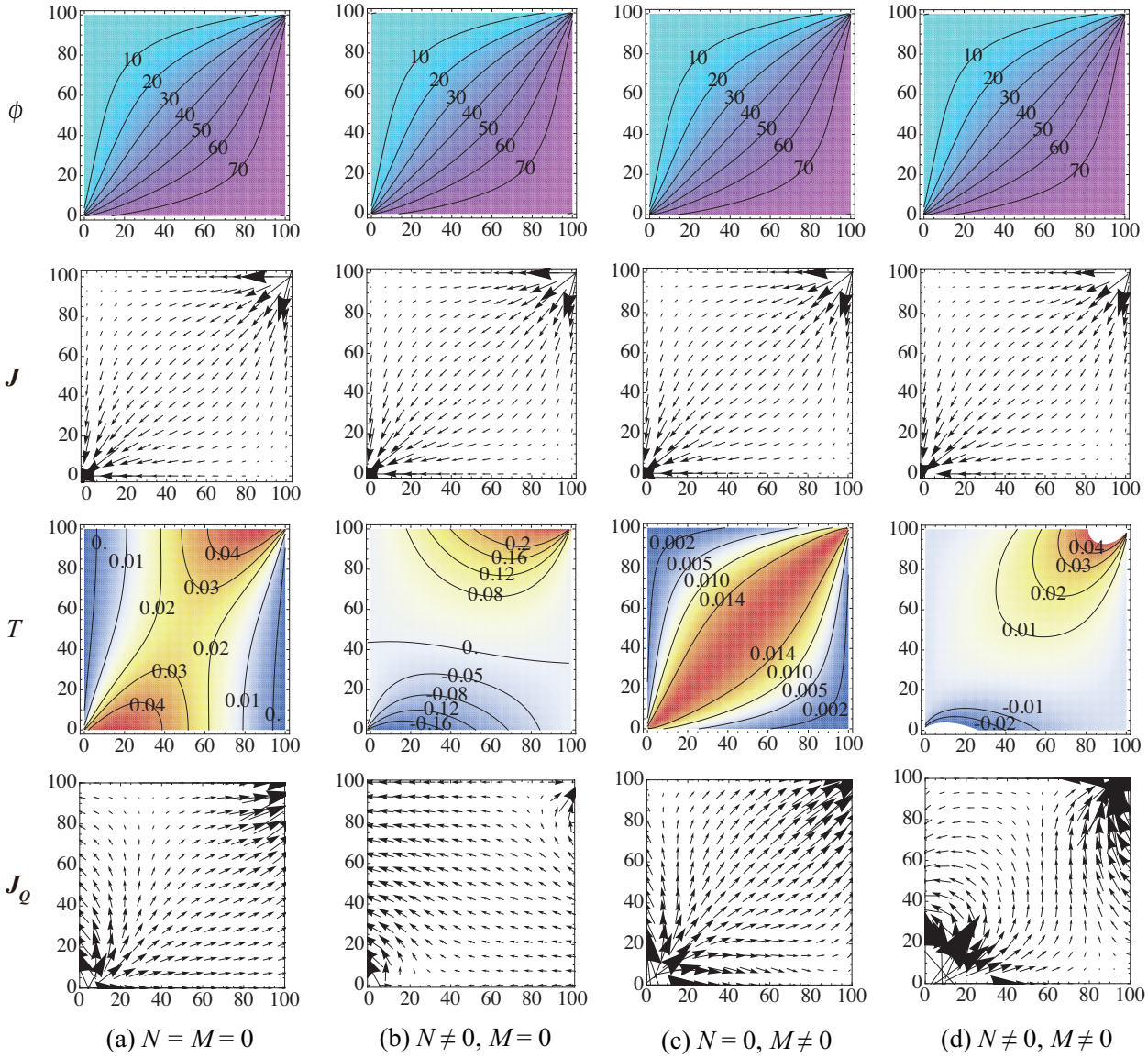

FIG. 5: (Color online) Distributions of ϕ, $\boldsymbol{J}$, T and $\boldsymbol{J_Q}$ at $B = 0.1$ T for (a) $N = M = 0$, (b) $N \neq 0,\ M = 0$, (c) $N = 0,\ M \neq 0$ and (d) $N \neq 0,\ M \neq 0$. (The data in (d) is the reproduction of Fig. 3 (c).) The ϕ-contours are labeled in the unit of nV. The labels for the T-contours indicate differences from $T_{\rm left} = T_{\rm right} = 40$ mK in the unit of μK.

$M < 0$ and $\partial_x \widetilde{T} > 0$ at the boundaries.

Finally, with $N \neq 0$ and $M \neq 0$, we obtain the distributions shown in Fig. 5 (d), which is the same as Fig. 3 (c) but re-presented for comparison. Since the third term in Eq. (14c) reduces $\partial_y \widetilde{T}$, a cooled area becomes smaller than that for $N \neq 0,\ M = 0$.

The distributions of ϕ and $\boldsymbol{J}$ remain unaltered throughout Fig. 5 (a)–(d), despite the change in the boundary condition (14c). This is because they are basically decoupled from the thermoelectric and thermomagnetic effects in the present situation, as demonstrated in section III A.

C. Threshold magnetic field for the cooling

In this section, we show that the cooled area is generated, in principle, by an arbitrarily small magnetic field; we can always find a cooled area if we can approach indefinitely close to the left-bottom corner. In practice, however, the minimum distance from the corner is limited by a certain physical length scale (obviously, the length, e.g., much smaller than the inter-atomic distance of the host crystal does not make sense), which sets a threshold for the magnetic field to generate the cooled area. In our discretized system used for the numerical calculation, the minimum distance is the separation between the grid (not the physical length scale but rather

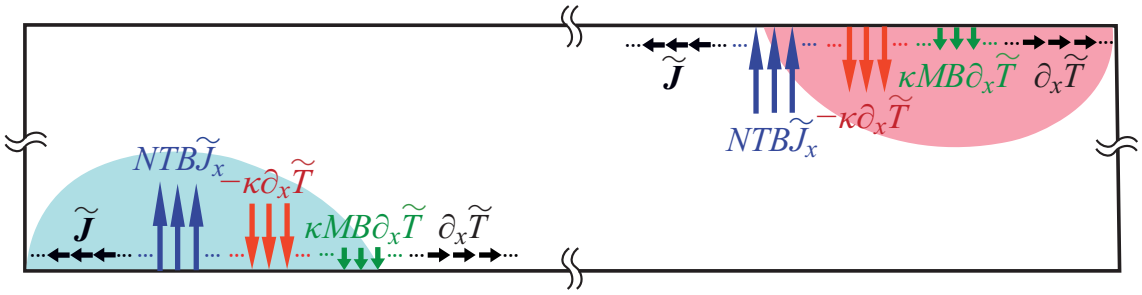

FIG. 6: (Color online) Schematic diagram showing the thermal current flow around the left-bottom and right-top corners. On the top and bottom boundaries, the total heat current vanishes, which is the sum of the heat current by the thermal diffusion ($-\kappa\partial_y\widetilde{T}$, red), the Ettingshausen ($NTB\widetilde{J}_x$, blue) effect and the Righi-Leduc ($\kappa MB\partial_x\widetilde{T}$, green) effect. The heat currents by the Ettingshausen and Righi-Leduc effects go upward and downward, respectively, since $\widetilde{J}_x < 0$, $\partial_x\widetilde{T} > 0$, $N < 0$, and $M < 0$. The right-top and left-bottom corners have temperatures higher and lower than the right and left boundaries, respectively, since $\partial_y\widetilde{T} > 0$.

an artificial distance), which determines the lowest magnetic field for the cooled areas to be observed on our grid points.

As described in section III A, Eqs. (4)–(7) and (9) are well-approximated by the simplified equations (11)–(13) and (15) for the present system. Equation (11) under the boundary conditions (15a) and (15c) can be solved analytically.[37] Although we have limited ourselves to the square sample thus far, analytical solutions are given more generally for rectangular samples ($L_x \neq L_y$ in Fig. 2). The electric field $\boldsymbol{E} = -\nabla\phi$ is given by

$$E_x = -E_0 e^{\gamma}\cos\vartheta, \tag{16a}$$
$$E_y = E_0 e^{\gamma}\sin\vartheta, \tag{16b}$$

with

$$\gamma = -4\theta_{\rm H}\sum_{n=1}^{\infty}\frac{1}{(2n-1)\pi}\frac{\sinh\left[(2n-1)\pi\eta\right]\cos\left[(2n-1)\pi\xi\right]}{\cosh\left[(2n-1)\frac{\pi\alpha}{2}\right]}, \tag{17}$$

$$\vartheta = 4\theta_{\rm H}\sum_{n=1}^{\infty}\frac{1}{(2n-1)\pi}\frac{\cosh\left[(2n-1)\pi\eta\right]\sin\left[(2n-1)\pi\xi\right]}{\cosh\left[(2n-1)\frac{\alpha\pi}{2}\right]}, \tag{18}$$

where we introduced the normalized coordinates $\xi = x/L_x$, $\eta = (y - L_y/2)/L_x$ and the aspect ratio $\alpha = L_y/L_x$. The constant E_0 in Eq. (16) is determined by the potential difference between the side boundaries $\Delta\phi = \phi_{\rm right} - \phi_{\rm left}$, the Hall angle $\theta_{\rm H}$ in Eq. (10) (or the magnetic field), and the aspect ratio α as

$$E_0 = \frac{\Delta\phi}{I(\theta_{\rm H},\alpha)L_x}, \tag{19}$$

$$I(\theta_{\rm H},\alpha) \equiv \int_0^1 \cos\left\{4\theta_{\rm H}\sum_{n=1}^{\infty}\frac{\sin\left[(2n-1)\pi\xi\right]}{(2n-1)\pi}\,\mathrm{sech}\left[(2n-1)\frac{\pi}{2}\alpha\right]\right\}d\xi \tag{20}$$

$$\simeq J_0\left(\frac{4\theta_{\rm H}}{\pi}\mathrm{sech}\frac{\alpha\pi}{2}\right), \tag{21}$$

with $J_0(x)$ the Bessel function of order zero.

From Eqs. (12) and (16), we have the electric current density,

$$J_x = -E_0\frac{\cos\theta_{\rm H}}{\rho}e^{\gamma}\cos(\vartheta - \theta_{\rm H}), \tag{22a}$$
$$J_y = E_0\frac{\cos\theta_{\rm H}}{\rho}e^{\gamma}\sin(\vartheta - \theta_{\rm H}), \tag{22b}$$
$$J = \sqrt{J_x^2 + J_y^2} = E_0 e^{\gamma}\frac{\cos\theta_{\rm H}}{\rho}. \tag{22c}$$

We obtain the total current $J_{\rm tot}$ by integrating J_x along an arbitrary axis in y-direction,

$$J_{\rm tot} = -L_x\int_{-\alpha/2}^{\alpha/2} J_x\left(\xi = \text{const.};\eta\right)d\eta = L_x E_0\frac{\cos(\theta_{\rm H})}{\rho}K(\theta_{\rm H},\alpha), \tag{23}$$

$$K(\theta_{\rm H},\alpha) \equiv \alpha\int_0^1\cos\left(4\theta_{\rm H}\sum_{n=1}^{\infty}(-1)^{n-1}\frac{\cosh\left[(2n-1)\frac{\alpha\pi}{2}\eta'\right]}{(2n-1)\pi}\mathrm{sech}\left[(2n-1)\frac{\alpha\pi}{2}\right] - \theta_{\rm H}\right)d\eta'. \tag{24}$$

For $\alpha = 1$ (square sample), it can be shown, to an extremely good approximation, that $K(\theta_{\rm H}, 1) \simeq I(\theta_{\rm H}, 1)$, which monotonically decreases with increasing $\theta_{\rm H}$ from 1 at $\theta_{\rm H} = 0$ to 0.847 at $\theta_{\rm H} = \pi/2$. Therefore we have

$$J_{\rm tot}(\alpha = 1) \simeq \frac{\Delta\phi \cos(\theta_{\rm H})}{\rho}. \tag{25}$$

We introduce here the polar coordinates (r, φ), where $r = \sqrt{x^2 + y^2}$ and $\varphi = \tan^{-1}(y/x)$, with the origin located at the left-bottom corner of the system as shown in Fig. 1 (b), noting that the current J is nearly isotropic in the vicinity of the corner as can be seen in Figs. 4 (c) and 4 (d). Using the polar coordinate notation for the temperature gradient, $\tau_r \equiv \partial_r T$ and $\tau_\varphi \equiv r^{-1}\partial_\varphi T$, the Poisson equation (13) is written as

$$\nabla \cdot \nabla T = \frac{1}{r}\frac{\partial}{\partial r}(r\tau_r) + \frac{1}{r}\frac{\partial}{\partial \varphi}\tau_\varphi = -\frac{\rho}{\kappa}J^2. \tag{26}$$

Since we find that $\tau_r \ll \tau_\varphi$ in the vicinity of the corner $r = 0$ in our numerical result, we can neglect the first term in Eq. (26). Thus, we can express the gradient τ_φ at the isothermal boundary ($\varphi = \pi/2$) with a small r by integrating Eq. (26) as,

$$\tau_\varphi\left(\frac{\pi}{2}, r\right) = \tau_\varphi|_{\varphi=0} - \frac{\rho}{\kappa}\int_0^{\pi/2} rJ^2 d\varphi. \tag{27}$$

Since J is nearly isotropic around the origin, we can replace J in the integral by J_x at the bottom boundary, $J|_{\varphi=0} = -J_x|_{y=0} \equiv J(r)$ (note that $J_x < 0$ and $J_y = 0$ at the bottom boundary). With this approximation, we obtain

$$\tau_\varphi\left(\frac{\pi}{2}, r\right) = \tau_\varphi|_{\varphi=0} - \frac{\rho}{\kappa}\frac{\pi}{2} rJ(r)^2. \tag{28}$$

Noting that M is not essential for the cooling effect (see Sec. III B), we assume $M = 0$ in Eq. (14c) for simplicity, to obtain

$$\tau_\varphi|_{\varphi=0} = \partial_y T|_{y=0} = -\frac{NTB}{\kappa}J(r). \tag{29}$$

Using Eq. (29) in Eq. (28), we have

$$\tau_\varphi\left(\frac{\pi}{2}, r\right) = -\frac{NTB}{\kappa}J(r) - \frac{\rho}{\kappa}\frac{\pi}{2} rJ(r)^2. \tag{30}$$

As illustrated in Fig. 7, temperatures lower than $T_{\rm left} = T(\varphi = \pi/2)$ emerge if $\tau_\varphi(\pi/2, r) > 0$, namely if

$$B > \frac{\pi}{2}\frac{\rho}{(-N)T} rJ(r) = \frac{\pi}{2}\frac{E_0 \cos\theta_{\rm H}}{(-N)T} re^{\gamma(r)}, \tag{31}$$

with $\gamma(r) \equiv \gamma(\xi = r/L_x, \eta = 0)$, and we used $N < 0$ in the derivation. As will be shown below, the right-hand side tends to 0 with $r \to 0$, although the current $J(r)$ diverges with $r \to 0$ (see Fig. 4). On the bottom boundary, we have from Eq. (17),

$$\gamma(r) = 4\theta_{\rm H}\left(\frac{1}{2\pi}\ln\left[\cot\left(\frac{\pi r}{2L_x}\right)\right] - \sum_{n=1}^{\infty}\frac{\cos\left[(2n-1)\pi\frac{r}{L_x}\right]}{(2n-1)\pi}\left\{1 - \tanh\left[(2n-1)\frac{\alpha\pi}{2}\right]\right\}\right). \tag{32}$$

The second term in the large round brackets is less than 0 for $r \to 0$, and thus from Eq. (22c),

$$J(r) < E_0\frac{\cos\theta_{\rm H}}{\rho}\exp\left\{\frac{2\theta_{\rm H}}{\pi}\ln\left[\cot\left(\frac{\pi r}{2L_x}\right)\right]\right\} = E_0\frac{\cos\theta_{\rm H}}{\rho}\left[\left(\frac{\pi r}{2L_x}\right)^{-\frac{2\theta_{\rm H}}{\pi}} + O(r)\right]. \tag{33}$$

Since $0 < 2\theta_{\rm H}/\pi < 1$, we have $rJ(r) \to 0$ for $r \to 0$.

With a fixed B, an area within the distance r from the left-bottom corner becomes colder than the isothermal boundary ($\varphi = \pi/2$) for r satisfying Eq. (31). Alternatively, for a fixed r (~ 0), Eq. (31) gives a threshold magnetic field for the position r to become colder than the isothermal boundary, (which can be made, in principle, arbitrarily small by letting $r \to 0$). Practical thresholds for the numerical calculation is given by the mesh spacing d. By setting $r = d = 0.1$ μm, we have a threshold magnetic field 0.03 T, which is consistent with our numerical results for $B = 0.03$ T (not shown).

IV. DISCUSSION

We have shown that the electron temperature can be cooled down by a dc electric current with an arbitrarily small magnetic field. The emergence of the cooled area is qualitatively consistent with the cooling inferred by the experimentally observed sign reversal of the Nernst signal[20] described in Introduction. We suspect, however, that the cooling mechanism demonstrated in the present study may not be the complete explanation for the experimental observation for several reasons.

First, the calculated temperature decrement is extremely small, order of 10^{-2} μK. It is rather unlikely that the effect caused by such a small temperature change can be experimentally detected. Although we believe that the present study captures the essence of the current-induced cooling, for more quantitative comparison with the experiment, it will be necessary to alter our boundary conditions to reflect the experimental conditions more precisely. Above all, we set the temperature of boundaries immediately to the left and right of the "heater section" fixed, while in the experiment the temperature is fixed at the left and right contact pads (hatched rectangles in Fig. 1(a)) separated $\sim$300 μm away from the heater section (the region below the front gate depicted by the gray rectangle in Fig. 1(a)). It seems plausible to

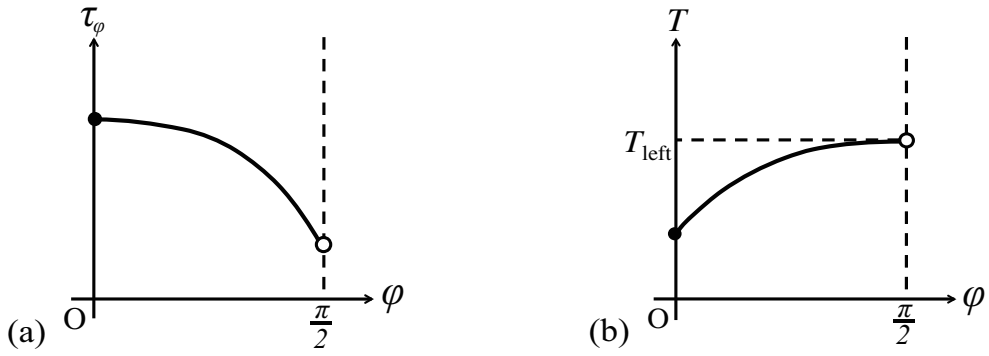

FIG. 7: Schematic illustration of the φ-dependences of (a) $\tau_\varphi = r^{-1}\partial_\varphi T$ and (b) T around the left-bottom corner, namely the origin of the polar coordinates. The points at $\varphi = 0$ (solid circle) and $\varphi = \pi/2$ (open circle) correspond to the bottom and the left edges, respectively. $\tau_\varphi(\varphi = 0) > 0$ and $T(\varphi = \pi/2) = T_{\rm left}$ have fixed values determined by the boundary conditions. Note that τ_φ decreases with φ, following Eq. (31). If $\tau_\varphi(\varphi = \pi/2) > 0$, T increases with φ near the left edge, ensuring the presence of the area colder than $T_{\rm left}$.

expect from the mechanism described in Sec. III that the separation allows larger variation of the temperature at the left-bottom corner of the heater section.

The fixed potential difference between the right and left boundaries $\Delta\phi$ is also at variance with the experiment, in which the total current $J_{\rm tot}$ is fixed. According to Eqs. (10) and (25), $J_{\rm tot}$ decreases with B if $\Delta\phi$ is kept constant. We can envisage a larger temperature change if we increase $\Delta\phi$ with B to keep $J_{\rm tot}$ constant as in the experiment. (We found difficulty, however, in the convergence of the numerical calculation if we set a larger value for $\Delta\phi$.)

So far, our calculation is limited to rather small magnetic field ($B \leq 0.2$ T) for technical reasons, especially for the bad convergence of the calculation. Noting that both the temperature decrement and the area of the cooled region increase with increasing magnetic field (see Fig. 3), we can expect much more pronounced cooling effect if we can extend our calculation to larger magnetic field.

Second, the sign reversal (corresponding to the appearance of the cooled area) was observed only when the magnetic field was large enough ($B > 1.8$ T) and only for the value of $V_{\rm g}$ at which electrons occupy less than half of the topmost Landau level (see Fig. 1 (c)). This can be related to the magnitude and the sign of the Ettingshausen coefficient NT, or equivalently, to those of the Nernst coefficient N. (Note that the Ettingshausen and Nernst coefficients are related by the Kelvin-Onsager relation.) As mentioned earlier, we used, in the present calculation, the value of $N(< 0)$ at $B = 0$ for simplicity, neglecting the B-dependence. In reality, the magnitude $|N|$ decreases with B, until the Landau levels are clearly resolved. In a quantizing magnetic field, $|N|$ again takes a large value when the Fermi energy E_F lies in a (disorder broadened) Landau level, with the sign of N alternating depending on whether E_F is below or above the center of the Landau level, namely, whether the energy derivative of the density of states is positive (electron-like) or negative (hole-like).[5,40] It can readily be seen from the discussion in Sec. III that the cold and hot areas appearing in the left-bottom and right-top corners, respectively, interchange their roles when the sign of N is inverted. The conditions for B and V_g mentioned above thus can be interpreted as the condition that N possesses a large enough magnitude (for the Ettingshausen effect to have sufficient strength) and the appropriate sign (so that the cooled area is generated on the side adjacent to the main Hall bar), respectively.

Third, in a 2DEG in the transition region between two adjacent quantum Hall states, the current is carried by both the bulk extended state of the topmost Landau level and the edge states from lower Landau levels. Although the edge states can have significant impact on the distributions of the electric and heat currents,[41] and hence on the temperature distribution, our calculation amounts to neglecting the edge states altogether.

Apparently, much improvement has to be made to quantitatively explain the experiment motivated our study. We believe, however, that our simplified approach has been advantageous to pinpoint the very essence of the cooling mechanism.

V. CONCLUSIONS

We have investigated the temperature distribution induced by a dc current in a 2DEG subjected to a perpendicular magnetic field, surrounded by the isopotential-isothermal (left and right) and insulated-adiabatic (top and bottom) boundaries (Fig. 1 (b), Fig. 2). By numerically solving the nonlinear Poisson equations (4) and (6), we have demonstrated that an area having the temperature lower than the isothermal boundaries (kept at 40 mK) appears in the vicinity of one of the corners where the electric current density is highly concentrated. The cooling is ascribed to the Ettingshausen effect, which

pumps the heat away from the adiabatic boundary. The adiabatic condition for the boundary (Eq. (8c)) requires the temperature gradient to be generated, with the resulting thermal diffusion canceling out the thermal current due to the Ettingshausen effect. We have shown that, owing to the temperature gradient, the cooled area emerges with an arbitrarily small magnetic field, although the area shrinks within closer proximity of the corner with decreasing magnetic field.

Although the present study is motivated by the recent experiment,[20] the calculated temperature decrement ($\sim 10^{-2}$ μK) is small and the relation of the present mechanism to the experiment remains rather unclear. Nevertheless, the confirmation of the presence of the counterintuitive current-induced cooling effect, as well as the identification of the mechanism responsible for the effect, is of importance in its own right, and underlines the complication brought about by the thermoelectric and thermomagnetic effects.

Acknowledgments

The present authors are grateful to Prof. A. Kamitani for valuable comments and thank Prof. H. Okumura for his advice on derivation of the nonlinear Poisson equations. The work is supported by a Grant-in-Aid for Scientific Research (B) No. 20340101 as well as by the Izumi Science and Technology Foundation and by NINS program for cross-disciplinary study (NIFS10KEIN0160) and by the National Institutes of Natural Sciences undertaking Forming Bases for Interdisciplinary and International Research through Cooperation Across Fields of Study and Collaborative Research Program No. NIFS08KEIN0091.

APPENDIX A: DERIVATION OF THE NONLINEAR POISSON EQUATIONS (4) AND (6)

In this Appendix, we present, for the self-containedness, the derivation of the nonlinear Poisson equations (4) and (6) from the transport equations (1) and (2) in the steady-state. We basically follow the prescription presented in Refs. 26 and 42. See also Ref. 1.

Taking account of the steady-state conditions

$$\nabla \cdot \boldsymbol{J} = 0 \tag{A1}$$

and

$$\nabla \cdot \boldsymbol{J_U} = \nabla \cdot (\boldsymbol{J_Q} + \phi \boldsymbol{J}) = 0, \tag{A2}$$

we take the divergence of Eq. (1):

$$\begin{aligned} -\nabla^2\phi =& \nabla \cdot [\rho \boldsymbol{J} + R\boldsymbol{B} \times \boldsymbol{J} + \alpha \nabla T + N\boldsymbol{B} \times \nabla T] \\ =& \nabla\rho \cdot \boldsymbol{J} + \nabla R \cdot (\boldsymbol{B} \times \boldsymbol{J}) + R[\nabla \cdot (\boldsymbol{B} \times \boldsymbol{J})] \\ &+ \nabla\alpha \cdot \nabla T + \alpha \nabla^2 T \\ &+ \nabla N \cdot (\boldsymbol{B} \times \nabla T) + N[\nabla \cdot (\boldsymbol{B} \times \nabla T)]. \end{aligned} \tag{A3}$$

Because, under the temperature gradient ∇T, an arbitrary transport coefficient X depends on (x, y) through its temperature dependence, the gradient of X can be expressed as

$$\nabla X = \frac{dX}{dT} \nabla T. \tag{A4}$$

We thus can rewrite Eq. (A3) as follows:

$$\begin{aligned} -\nabla^2\phi =& \frac{d\rho}{dT}(\boldsymbol{J} \cdot \nabla T) \\ &+ \frac{dR}{dT}[\nabla T \cdot (\boldsymbol{B} \times \boldsymbol{J})] + R[\nabla \cdot (\boldsymbol{B} \times \boldsymbol{J})] \\ &+ \frac{d\alpha}{dT}(\nabla T)^2 + \alpha \nabla^2 T \\ &+ \frac{dN}{dT}[\nabla T \cdot (\boldsymbol{B} \times \nabla T)] + N[\nabla \cdot (\boldsymbol{B} \times \nabla T)]. \end{aligned} \tag{A5}$$

Using formulas for vector operation, Eq. (A5) becomes

$$\begin{aligned} -\nabla^2\phi =& \frac{d\rho}{dT}(\boldsymbol{J} \cdot \nabla T) + \frac{dR}{dT}[\nabla T \cdot (\boldsymbol{B} \times \boldsymbol{J})] \\ &+ R[\boldsymbol{J} \cdot (\nabla \times \boldsymbol{B}) - \boldsymbol{B} \cdot (\nabla \times \boldsymbol{J})] \\ &+ \frac{d\alpha}{dT}(\nabla T)^2 + \alpha \nabla^2 T \\ &+ N \nabla T \cdot (\nabla \times \boldsymbol{B}). \end{aligned} \tag{A6}$$

Using further the Maxwell equation $\nabla \times \boldsymbol{B} = \mu \boldsymbol{J} + \epsilon\mu(d\boldsymbol{E}/dt) = 0$ in the steady state, omitting the negligibly small term μJ, Eq. (A6) becomes

$$\begin{aligned} -\nabla^2\phi =& \frac{d\rho}{dT}(\boldsymbol{J} \cdot \nabla T) \\ &+ \frac{dR}{dT}[\nabla T \cdot (\boldsymbol{B} \times \boldsymbol{J})] - R[\boldsymbol{B} \cdot (\nabla \times \boldsymbol{J})]. \\ &+ \frac{d\alpha}{dT}(\nabla T)^2 + \alpha \nabla^2 T. \end{aligned} \tag{A7}$$

Here we calculate $\nabla \times \boldsymbol{J}$ from Eq. (1) under the conditions (A1) and (A2). The rotation of Eq. (1) gives

$$\begin{aligned} 0 =& -\nabla \times \nabla\phi \\ =& \nabla \times [\rho \boldsymbol{J} + R\boldsymbol{B} \times \boldsymbol{J} + \alpha \nabla T + N\boldsymbol{B} \times \nabla T] \\ =& \frac{d\rho}{dT}(\nabla T \times \boldsymbol{J}) + \rho(\nabla \times \boldsymbol{J}) \\ &+ (\boldsymbol{J} \cdot \nabla)(R\boldsymbol{B}) - (R\boldsymbol{B} \cdot \nabla)\boldsymbol{J} - \boldsymbol{J}[\nabla \cdot (R\boldsymbol{B})] \\ &+ R\boldsymbol{B}(\nabla \cdot \boldsymbol{J}) \\ &+ \frac{d\alpha}{dT}(\nabla \times \nabla T) + \alpha(\nabla \times \nabla T) \\ &+ (\nabla T \cdot \nabla)(N\boldsymbol{B}) - (N\boldsymbol{B} \cdot \nabla)\nabla T \\ &- \nabla T[(\nabla \cdot (N\boldsymbol{B})] + N\boldsymbol{B}(\nabla \cdot \nabla T) \\ =& \frac{d\rho}{dT}(\nabla T \times \boldsymbol{J}) + \rho(\nabla \times \boldsymbol{J}) \\ &+ \frac{dR}{dT}(\boldsymbol{J} \cdot \nabla T)\boldsymbol{B} + \left[N\nabla^2 T + \frac{dN}{dT}(\nabla T)^2\right]\boldsymbol{B}. \end{aligned} \tag{A8}$$

We thus obtain

$$\nabla \times \boldsymbol{J} = -\frac{1}{\rho}\left\{\frac{d\rho}{dT}(\nabla T \times \boldsymbol{J}) + \left[\frac{dR}{dT}(\boldsymbol{J}\cdot\nabla T) + N\nabla^2 T + \frac{dN}{dT}(\nabla T)^2\right]\boldsymbol{B}\right\}. \tag{A9}$$

By substituting Eq. (A9) into Eq. (A7), we obtain the following equation:

$$\begin{aligned}-\nabla^2\phi =& \frac{d\rho}{dT}(\boldsymbol{J}\cdot\nabla T) \\ &+ \frac{dR}{dT}[\nabla T\cdot(\boldsymbol{B}\times\boldsymbol{J})] + \frac{R}{\rho}\frac{d\rho}{dT}[\boldsymbol{B}\cdot(\nabla T\times\boldsymbol{J})] \\ &+ \frac{RB^2}{\rho}\left[\frac{dR}{dT}(\boldsymbol{J}\cdot\nabla T) + N\nabla^2 T + \frac{dN}{dT}(\nabla T)^2\right] \\ &+ \frac{d\alpha}{dT}(\nabla T)^2 + \alpha\nabla^2 T \\ =& \left(\frac{d\alpha}{dT} + \frac{RB^2}{\rho}\frac{dN}{dT}\right)(\nabla T)^2 \\ &- \left(\frac{R}{\rho}\frac{d\rho}{dT} - \frac{dR}{dT}\right)[\nabla T\cdot(\boldsymbol{B}\times\boldsymbol{J})] \\ &+ \left(\frac{d\rho}{dT} + \frac{RB^2}{\rho}\frac{dR}{dT}\right)(\boldsymbol{J}\cdot\nabla T) \\ &+ \left(\alpha + \frac{RNB^2}{\rho}\right)\nabla^2 T. \end{aligned} \tag{A10}$$

By substituting Eq. (6) (to be derived below) into Eq. (A10), we obtain Eq. (4).

Next, we derive the Poisson equation for T, Eq. (6). We obtain the following equation from the divergence of $\boldsymbol{J_U}$ in Eq. (3) using Eqs. (2), (A1), and (A2):

$$\begin{aligned}&\nabla\cdot(\phi\boldsymbol{J}) + \nabla\cdot(\alpha T\boldsymbol{J}) + \nabla\cdot[NT(\boldsymbol{B}\times\boldsymbol{J})] \\ &\quad - \nabla\cdot(\kappa\nabla T) + \nabla\cdot[\kappa M(\boldsymbol{B}\times\nabla T)] \\ &= \nabla\phi\cdot\boldsymbol{J} + \nabla\alpha\cdot(T\boldsymbol{J}) + \alpha\nabla T\cdot\boldsymbol{J} \\ &\quad + (T\nabla N + N\nabla T)\cdot(\boldsymbol{B}\times\boldsymbol{J}) + NT[\nabla\cdot(\boldsymbol{B}\times\boldsymbol{J})] \\ &\quad - \nabla\kappa\cdot\nabla T - \kappa\nabla^2 T + (M\nabla\kappa + \kappa\nabla M)\cdot(\boldsymbol{B}\times\nabla T) \\ &\quad + \kappa M[\nabla\cdot(\boldsymbol{B}\times\nabla T)] = 0. \end{aligned} \tag{A11}$$

Using Eq. (A4), we have

$$\begin{aligned}&\nabla\phi\cdot\boldsymbol{J} + \left(T\frac{d\alpha}{dT} + \alpha\right)(\nabla T\cdot\boldsymbol{J}) \\ &\quad + \left(T\frac{dN}{dT} + N\right)[\nabla T\cdot(\boldsymbol{B}\times\boldsymbol{J})] + NT[\nabla\cdot(\boldsymbol{B}\times\boldsymbol{J})] \\ &\quad - \frac{d\kappa}{dT}(\nabla T)^2 - \kappa\nabla^2 T \\ &\quad + \left(M\frac{d\kappa}{dT} + \kappa\nabla\frac{dM}{dT}\right)[\nabla T\cdot(\boldsymbol{B}\times\nabla T)] \\ &\quad + \kappa M[\nabla\cdot(\boldsymbol{B}\times\nabla T)] = 0. \end{aligned} \tag{A12}$$

Using again formulas for vector operation, we rewrite the above equation as,

$$\begin{aligned}&\nabla\phi\cdot\boldsymbol{J} + \left(T\frac{d\alpha}{dT} + \alpha\right)(\nabla T\cdot\boldsymbol{J}) \\ &\quad + \left(T\frac{dN}{dT} + N\right)[\nabla T\cdot(\boldsymbol{B}\times\boldsymbol{J})] \\ &\quad + NT[\boldsymbol{J}\cdot(\nabla\times\boldsymbol{B}) - \boldsymbol{B}\cdot(\nabla\times\boldsymbol{J})] \\ &\quad - \frac{d\kappa}{dT}(\nabla T)^2 - \kappa\nabla^2 T \\ &\quad + \kappa M[\nabla T\cdot(\nabla\times\boldsymbol{B})] = 0, \end{aligned} \tag{A13}$$

which reduces, with the Maxwell equation $\nabla\times\boldsymbol{B} = 0$, to

$$\begin{aligned}\kappa\nabla^2 T =& \nabla\phi\cdot\boldsymbol{J} + \left(T\frac{d\alpha}{dT} + \alpha\right)(\nabla T\cdot\boldsymbol{J}) \\ &+ \left(T\frac{dN}{dT} + N\right)[\nabla T\cdot(\boldsymbol{B}\times\boldsymbol{J})] \\ &- NT[\boldsymbol{B}\cdot(\nabla\times\boldsymbol{J})] - \frac{d\kappa}{dT}(\nabla T)^2. \end{aligned} \tag{A14}$$

We substitute Eq. (1) into the above equation and obtain

$$\begin{aligned}\kappa\nabla^2 T =& -[\rho\boldsymbol{J} + R(\boldsymbol{B}\times\boldsymbol{J}) + \alpha\nabla T + N(\boldsymbol{B}\times\nabla T)]\cdot\boldsymbol{J} \\ &+ \left(T\frac{d\alpha}{dT} + \alpha\right)(\nabla T\cdot\boldsymbol{J}) \\ &+ \left(T\frac{dN}{dT} + N\right)[\nabla T\cdot(\boldsymbol{B}\times\boldsymbol{J})] \\ &- NT[\boldsymbol{B}\cdot(\nabla\times\boldsymbol{J})] - \frac{d\kappa}{dT}(\nabla T)^2 \\ =& -\rho J^2 + T\frac{d\alpha}{dT}(\nabla T\cdot\boldsymbol{J}) \\ &+ \left(T\frac{dN}{dT} + 2N\right)[\nabla T\cdot(\boldsymbol{B}\times\boldsymbol{J})] \\ &- NT\,[\boldsymbol{B}\cdot(\nabla\times\boldsymbol{J})] - \frac{d\kappa}{dT}(\nabla T)^2. \end{aligned} \tag{A15}$$

By substituting Eq. (A9) into Eq. (A15), we arrive at Eq. (6).

[1] T. Harman and J. M. Honig, *Thermoelectric and Thermomagnetic Effects and Applications* (McGraw-Hill, New York, 1967).

[2] V. Zlatic and A. C. Hewson, eds., *Properties and Applications of Thermoelectric Materials* (Springer, Dordrecht, 2009).

[3] D. M. Rowe, ed., *Thermoelectrics handbook : macro to nano* (CRC Taylor & Francis, Boca Raton, 2006).

[4] B. L. Gallagher and P. N. Butcher, "Handbook on semiconductors vol. 1," (Elsevier, Amsterdam, 1992) p. 817.

[5] R. Fletcher, Semicond. Sci. Technol. **14**, R1 (1999).

[6] X. Ying, V. Bayot, M. B. Santos, and M. Shayegan, Phys. Rev. B **50**, R4969 (1994).

[7] W. E. Chickering, J. P. Eisenstein, and J. L. Reno, Phys. Rev. Lett. **103**, 046807 (2009).

[8] S. Goswami, C. Siegert, M. Baenninger, M. Pepper, I. Farrer, and D. A. Ritchie, Phys. Rev. Lett. **103**, 026602 (2009).

[9] K. Yang and B. I. Halperin, Phys. Rev. B **79**, 115317 (2009).

[10] W. E. Chickering, J. P. Eisenstein, L. N. Pfeiffer, and K. W. West, Phys. Rev. B **81**, 245319 (2010).

[11] D. L. Bergman and V. Oganesyan, Phys. Rev. Lett. **104**, 066601 (2010).

[12] K. Behnia, M.-A. Méasson, and Y. Kopelevich, Phys. Rev. Lett. **98**, 166602 (2007).

[13] K. Behnia, L. Balicas, and Y. Kopelevich, Science **317**, 1729 (2007).

[14] A. Endo and Y. Iye, to appear in Proc. 30th Int. Conf. Phys. of Semicond. (2011).

[15] K. Yoshihiro, J. Kinoshita, K. Inagaki, C. Yamanouchi, T. Endo, Y. Murayama, M. Koyanagi, A. Yagi, J. Wakabayashi, and S. Kawaji, Phys. Rev. B **33**, 6874 (1984).

[16] N. R. Cooper, B. I. Halperin, and I. M. Ruzin, Phys. Rev. B **55**, 2344 (1997).

[17] H. Akera and H. Suzuura, J. Phys. Soc. Jpn. **74**, 997 (2005).

[18] T. Ise, H. Akera, and H. Suzuura, J. Phys. Soc. Jpn. **74**, 259 (2005).

[19] Y. Komori and T. Okamoto, Phys. Rev. B **71**, 113306 (2005).

[20] K. Fujita, A. Endo, S. Katsumoto, and Y. Iye, Physica E **42**, 1030 (2010).

[21] S. Maximov, M. Gbordzoe, H. Buhmann, L. W. Molenkamp, and D. Reuter, Phys. Rev. B **70**, 121308 (2004).

[22] M. Jonson and S. M. Girvin, Phys. Rev. B **29**, 1939 (1984).

[23] H. Oji, Phys. Rev. B **29**, 3148 (1984).

[24] R. Fletcher, J. C. Maan, K. Ploog, and G. Weimann, Phys. Rev. B **33**, 7122 (1986).

[25] We surmise that the insulated-adiabatic condition for the top and bottom boundaries, obvious when the heater section is isolated as in Fig. 1 (b), approximates the boundary condition for the heater section embedded in the device as in Fig. 1 (a) fairly well. In the experiment, only the current contacts (hatched rectangles in Fig. 1(a)) are connected to an external current source; the other contacts are electrically isolated, restricting the electric current from flowing into the main (vertical) Hall bar. Therefore the vast majority of the large heating electric current Ih, and hence the resulting heat current due to the carrier diffusion, is limited to the horizontal bar. Since we neglect the phonon contribution to the heat current (see below), the top and bottom edges of the heater section effectively act as insulated and adiabatic boundaries.

[26] H. Okumura, S. Yamaguchi, H. Nakamura, K. Ikeda, and K. Sawada, Proceedings of ICT98: 17th International Conference on Thermoelectrics, 1998 , 89 (1998).

[27] L. D. Landau, E. M. Lifshitz, and L. P. Pitaevskii, *Electrodynamics of Continuous Media, 2nd ed.* (Pergamon, Oxford, 1984).

[28] T. Harman and J. M. Honig, J. Appl. Phys. **33**, 3178 (1962).

[29] H. B. Callen, *Thermodynamics* (John Wiley & Sons, New York, 1960).

[30] G. D. Smith, *Numerical Solution of Partial Differential Equations* (Oxford University Press, 1965).

[31] M. Metcalf, W. H. Press, S. A. Teukolsky, W. T. Vetterling, and B. P. Flannery, *Numerical Recipes in Fortran 90 vol. 2* (Cambridge University Press, 1996).

[32] N. Hirayama, A. Endo, K. Fujita, Y. Hasegawa, N. Hatano, H. Nakamura, R. Shirasaki, and K. Yonemitsu, Auxiliary Material.

[33] J. M. Ziman, *Electrons and Phonons* (Oxford University Press, Oxford, 1960).

[34] N. Hirayama, A. Endo, K. Fujita, Y. Hasegawa, N. Hatano, H. Nakamura, and R. Shirasaki, Comput. Phys. Commun. **182**, 90 (2011).

[35] N. Hirayama, A. Endo, K. Fujita, Y. Hasegawa, N. Hatano, H. Nakamura, R. Shirasaki, and K. Yonemitsu, to appear in J. Electron. Mater. (2011).

[36] R. F. Wick, J. Appl. Phys. **25**, 741 (1954).

[37] R. W. Rendell and S. M. Girvin, Phys. Rev. B **23**, 6610 (1981).

[38] J. Wakabayashi and S. Kawaji, J. Phys. Soc. Jpn. **44**, 1839 (1978).

[39] B. Neudecker and K. H. Hoffmann, Solid State Commun. **62**, 135 (1987).

[40] Note that N in the present paper corresponds to S_{xy}/B in Ref. 5.

[41] G. Granger, J. P. Eisenstein, and J. L. Reno, Phys. Rev. Lett. **102**, 086803 (2009).

[42] H. Okumura, `http://oku.edu.mie-u.ac.jp/~okumura/nernst/nernst.pdf` (2000), (in Japanese).